ACS Partner Journal

Journal of the American Society for Mass Spectrometry

pubs.acs.org/jasms

Article

Resolving Hidden Solution Conformations of Hemoglobin Using IMS-IMS on a Cyclic Instrument

Published as part of the Journal of the American Society for Mass Spectrometry virtual special issue "Focus: Next Generation Mass Spectrometry Omics Technologies".

Edie M. Sharon, Lucas W. Henderson, and David E. Clemmer*

Cite This: *J. Am. Soc. Mass Spectrom.* 2023, 34, 1559−1568

Read Online

ACCESS | Metrics & More | Article Recommendations | Supporting Information

ABSTRACT: Ion mobility spectrometry−mass spectrometry (IMS-MS) experiments on a cyclic IMS instrument were used to examine heterogeneous distributions of structures found in the 15+ to 18+ charge states of the hemoglobin tetramer (Hb). The resolving power of IMS measurements is known to increase with increasing drift-region length. This effect is not significant for Hb charge states as peaks were shown to broaden with increasing drift-region length. This observation suggests that multiple structures with similar cross sections may be present. To examine this hypothesis, selections of drift time distributions were isolated and subsequently reinjected into the mobility region for additional separation. These IMS-IMS experiments demonstrate that selected regions separate further upon additional passes around the drift cell, consistent with the idea that initial resolving power was limited due to the presence of many closely related conformations. Additional variable temperature electrospray ionization (vT-ESI) experiments were conducted to study how changing the solution temperature affects solution conformations. Some features in these IMS-IMS studies were observed to change similarly with solution temperature compared to features in the single IMS distribution. Other features changed differently in the selected mobility data, indicating that solution structures that were obscured upon IMS analysis because of the complex heterogeneity of the original distribution are discernible after reducing the number of conformers that are analyzed by further IMS analysis. These results illustrate that the combination of vT-ESI with IMS-IMS is useful for resolving and exploring conformer distributions and stabilities in systems that exhibit a large degree of structural heterogeneity.

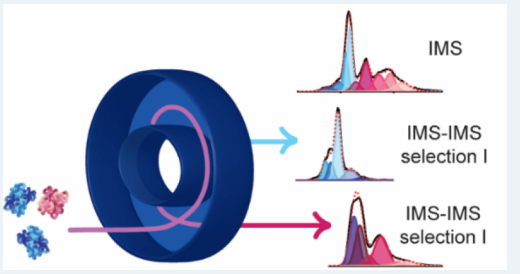

INTRODUCTION

Proteins regulate many biological functions related to wellness and disease[1−3] such as pathways for fighting off infections,[4] metabolism,[5,6] and the synthesis and degradation of other proteins.[7,8] These processes and others are made possible when chains of amino acids adopt properly folded (native) protein conformations that expose and shield specific residues, enabling function.[9−12] Understanding protein structure is therefore central to understanding biological function. To this end, many techniques for examining protein conformations have been developed including circular dichroism (CD)[13] and other spectroscopic strategies,[14−17] nuclear magnetic resonance (NMR)[18] and X-ray crystallography,[19] and mass spectrometry (MS),[20−23] among others. There are now over 200,000 protein structures available in the Protein Data Bank.[24] Most of these structures correspond to native folds because studies of non-native structures are often limited by the low abundances and transient lifetimes of these species.[25] Ion mobility spectrometry−mass spectrometry (IMS-MS) has emerged as a technique that is especially well suited for examining non-native conformations (as well as native conformers).[26,27] When combined with variable temperature (vT) electrospray ionization (ESI) sources,[28−32] IMS can provide information about the stabilities of states that are not readily accessible by other methods.[30] This technique has been used to examine conformers for individual proteins,[31,33−35] determine the stability of protein mixtures,[36] and derive detailed thermodynamics for native and non-native structures.[37] Additional IMS studies have extensively characterized the relationship between solution and gas-phase states,[38−44] thus providing insight about the role of solvent in establishing protein structures.[45−53] The possibilities for IMS measurements have expanded because of remarkable advances in technology[54] and numerous approaches are now available including linear drift tube IMS, linear and cyclic traveling wave

Received: January 30, 2023
Revised: May 31, 2023
Accepted: June 16, 2023
Published: July 7, 2023

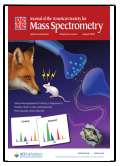

(TW) IMS,[55,56] field asymmetric IMS, differential mobility analysis, structures for lossless ion manipulations (SLIM),[57−59] and trapped IMS (TIMS).[60]

The commercial availability of cyclic IMS[61] allows access to an extended path length that can be varied based on the separation time during which ions traverse the circular drift cell. Longer path lengths increase the resolving power of the measurement,[56,62,63] enabling the resolution of otherwise indistinguishable conformers.[64−66] Additionally, cyclic drift regions enable higher order IMS^n separations which can be thought of as analogous to MS^n strategies based on differences in conformation with each IMS selection, rather than mass upon MS selection.[67,68] Previous studies from our laboratory and others, using home-built IMS-IMS instruments, illustrate improvements in the peak capacities of separations[69] as well as the isolation and activation of specific structures within the ensemble of conformational states.[70] In the study presented below and elsewhere, IMS-IMS experiments are conducted by ejecting a population of ions from the drift cell and subsequently reinjecting this population for further separation after the remaining ions have exited.[71−73] A visual representation of this process is presented in Scheme S1. This technique appears to mitigate the broadening effect that arises as similar conformers begin to separate with higher numbers of passes and allows for the study of populations of structures that remain obscured with a single IMS dimension.

The experiments reported below use these instrumental capabilities to probe the temperature dependence of populations of human hemoglobin (Hb) structures from solution. Hb is often referred to as a dimer of heterodimers because it consists of two α-subunits and two β-subunits, each associated with their own noncovalently bound heme group.[74] It is a model system for examining allosteric interactions because binding a single oxygen molecule to one of the hemoglobin monomers influences the interactions between other subunits, inducing long-range conformational changes that increase the favorability of oxygen binding at the other three heme groups.[75] This shift has traditionally been characterized as a two-state transition from the deoxygenated (T) structure to the oxygenated (R) structure,[76] but several studies provide evidence for additional structures including the R2,[77−79] RR2,[80] and R3[80] states among others,[81] indicating conformational heterogeneity that requires further characterization. Previous work from our research group has found four conformations in the ion mobility spectrum of the hemoglobin tetramer based on unique changes in abundance at elevated solution temperatures.[82] In this study, we observe an increased diversity of structural shifts in the tetramer which are discernible with the cyclic IMS instrument due to an increase in the path length of the mobility separation and the capability to isolate selected populations of ions.

EXPERIMENTAL SECTION

Sample Preparation. Human hemoglobin A (Sigma-Aldrich, St. Louis, MO) was prepared in water (LC-MS grade, Fisher Chemical, Fair Lawn, NJ) and buffer-exchanged into a solution of 100 mM ammonium acetate (pH 7.4) using a size exclusion chromatography spin column with a 6 kDa limit (Micro-Bio Spin 6, Bio-Rad Laboratories, Hercules, CA). Calibrant solutions of ubiquitin and β-lactoglobulin were prepared in 49:49:2 water/methanol/acetic acid and 200 mM ammonium acetate, respectively.

Variable-Temperature Electrospray Ionization. Electrospray emitters were made in house from borosilicate glass capillaries (Sutter Instrument, Novato, CA) pulled to a fine point (~1−2 μm) using a Flaming/Brown micropipette puller (Model P-97, Sutter Instrument, Novato, CA). Capillaries were loaded with sample solution and inserted into a custom variable temperature source described previously.[31] Briefly, the capillary was enclosed in a thermally conductive boron nitride ceramic block that also housed a cartridge heater. A thermocouple probe was attached to the block near the tip of the capillary and provided feedback that allowed the cartridge heater to modulate the solution temperature. A voltage was applied via a platinum wire inserted into the capillary (1−1.8 kV) in order to create electrospray droplets. The source was attached to a Waters Select Series Cyclic IMS instrument with the source interlocks in override. All instrument parameters are provided in the Supporting Information (SI) (Table S1).

Calibration. We include a detailed explanation of our calibration process for multipass and selected mobility distributions given the relative novelty of these measurements on the cyclic instrument. For all single pass experiments, calibration was performed based on previously described procedures.[83,84] Ubiquitin and β-lactoglobulin were used as calibrants. Calibrant samples were run using the same settings that were used in all single pass experiments for hemoglobin as described in Table S1. Mobility distributions were extracted in units of drift time. The separation time and eject and acquire time were subtracted from the total drift time so that only the injection time (10 ms) was used to generate a logarithmic calibration curve based on collision cross section values in nitrogen buffer gas.[84] All collision cross section values for single pass mobility experiments were determined from this curve which is included in the Supporting Information (Figure S1). The drift times for all selected mobility distributions were adjusted based on two criteria prior to calibration. First, the drift time for the most abundant peak from the selected spectrum was adjusted as necessary to align with the drift time of the most abundant peak in the corresponding single pass mobility spectrum. This adjustment assumes that the most abundant species in a specific drift time region exhibits the same mobility in both types of experiments. Second, the width of the selected mobility spectrum was adjusted so that the signal was contained within the drift time region selected from the corresponding single pass mobility spectrum. This adjustment helps correct for broadening due to diffusion and separation of additional conformations which would otherwise indicate the presence of structures with cross sections that are much larger or smaller than those of the original mobility distributions from which the selected distributions are derived. Examples of the effect of this adjustment are presented in Figure S2. Though analyte ions from multipass and IMS-IMS experiments have spent more time in the gas phase compared to calibrant ions, significant differences in drift time distributions (and subsequently in cross section values) are unlikely to occur on the time scale of these experiments as demonstrated previously.[85] For further discussion of potential activation as it pertains to these experiments, see Figure S3.

Data Analysis. IMS-MS data were extracted using TWIMExtract software (University of Michigan, Ann Arbor, MI)[86] and plotted using OriginPro2021 (OriginLab Corporation, Northhampton, MA). Mobility distributions were normalized and smoothed with a 5-point adjacent average

https://doi.org/10.1021/jasms.3c00032
J. Am. Soc. Mass Spectrom. 2023, 34, 1559−1568

filter. Distributions were modeled with Gaussian functions with the center and width of each peak held constant across all temperatures as described previously.[37] The number of peaks used to fit each charge state was increased until the fit converged to an R^2 of 0.95 or greater across all temperatures for three replicate experiments. A separate fit was created for each charge state and for each selection examined with IMS-IMS. Once the positions of the widths of each Gaussian in the model are established, we change only the abundances in modeling the data. Additional discussion regarding modeling of IMS-IMS data is provided in the SI. All mobility distributions are representative of a single experiment, and all relative abundance plots represent averaged results of triplicate experiments.

RESULTS AND DISCUSSION

Mass Spectra. Mass spectra of hemoglobin and temperature dependence of the observed species have been discussed previously,[82,87] so discussion of these data is limited to a brief summary. The mass spectrum of hemoglobin taken on the cyclic IMS instrument at a solution temperature of 24 °C is shown in Figure 1a. Peaks corresponding to the intact tetramer are observed alongside peaks corresponding to the dimer and monomer subunits. The dimer and monomer species increase in intensity at higher temperatures which indicates that the tetramer has begun to dissociate. This heterogeneity gives rise to an abundance of mobility data and, given the additional intricacy generated by selecting these data, the tetramer was chosen as the focus for the mobility experiments detailed below. Hereafter, any mention of hemoglobin can be assumed to refer to the tetramer. Hemoglobin is present at charge states ranging from 15+ to 17+ at 24 °C, although the 18+ charge state is also observed at higher solution temperatures. At temperatures above 60 °C, aggregation in the tip leads to loss of spray and signal, consistent with previous studies.[82] Representative mass spectra at various temperatures as well as plots of the average charge state of the tetramer and relative abundances of the tetramer and dimer as a function of temperature are provided in Figures S4−S6.

Comparison of vT-ESI Results to Prior Work. Ion mobility distributions for all four charge states of hemoglobin are shown in Figure 1. The data presented in Figure 1b were acquired previously[82] using a linear TW instrument (having a drift cell path length of 25.4 cm[88]), while the data presented in Figure 1c were acquired after a single pass through a 98 cm long cyclic drift cell. For these experiments, a pass around the drift tube will require a different amount of time for ions having different mobilities. When a distribution of ions has traveled around the entire circle, all species will have undergone a pass. In Figure 1, the difference in the number of Gaussian peaks required to model each data set is visually apparent. Prior data acquired on the linear instrument require three Gaussian curves to model the 15+ and 18+ charge states; the 16+ and 17+ charge states require two peaks. However, with the cyclic instrument, the 15+ and 18+ charge states each require eight Gaussians to model the data; the 16+ and 17+ charge states require seven and nine peaks, respectively. The increase in the number of peaks required to appropriately fit the mobility distributions indicates that additional conformations are present and can be resolved with the cyclic instrument, presumably as a result of the extended drift cell path length.

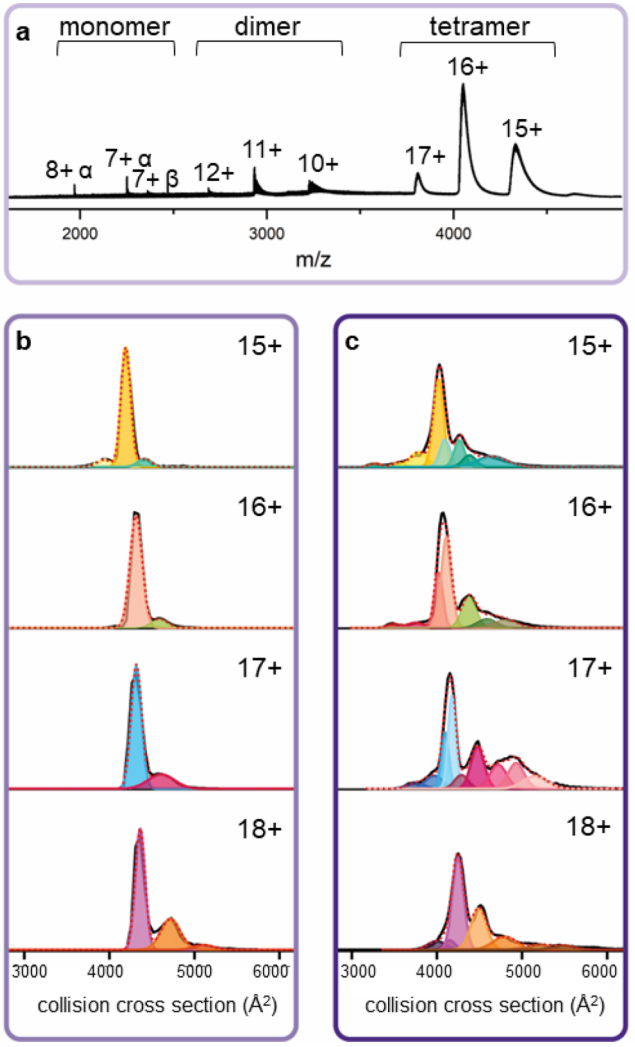

Figure 1. (a) Mass spectrum of hemoglobin. (b) IMS distributions for each charge state of the hemoglobin tetramer (15+ to 18+) recorded on a G2 IMS instrument with a mobility cell path length of 25.4 cm (see ref 39). (c) IMS distributions for each charge state of the hemoglobin tetramer (15+ to 18+) after a single pass through a cyclic IMS instrument with a mobility cell path length of 98 cm.

Multipass Separations. Previous experiments performed on a cyclic IMS instrument demonstrate that resolution increases for small molecules as the number of passes through the drift cell increases.[61,65,73] This effect is shown in Figure 2a for a mixture of three trisaccharides (melezitose, raffinose, and maltotriose) after undertaking various numbers of passes through the cyclic drift cell. These three compounds have the same mass and so are indistinguishable by mass spectrometry alone, but their isomeric nature allows them to be separated with ion mobility as previously demonstrated.[89] After a single pass, only two peaks are observed in the mobility spectrum, but adding an additional pass separates a third peak so that all three isomers are represented. Increasing the number of passes further separates these three peaks and baseline separation is achieved after six passes. Beyond this point, the "wrap-around" phenomenon occurs where faster ions catch up to slower-moving ions and prevent accurate peak identification.[61] The resolving power of each peak in these distributions is provided in Table S2 and plotted in Figure S7 which demonstrates how this value steadily increases with the number of passes.

https://doi.org/10.1021/jasms.3c00032
J. Am. Soc. Mass Spectrom. 2023, 34, 1559−1568

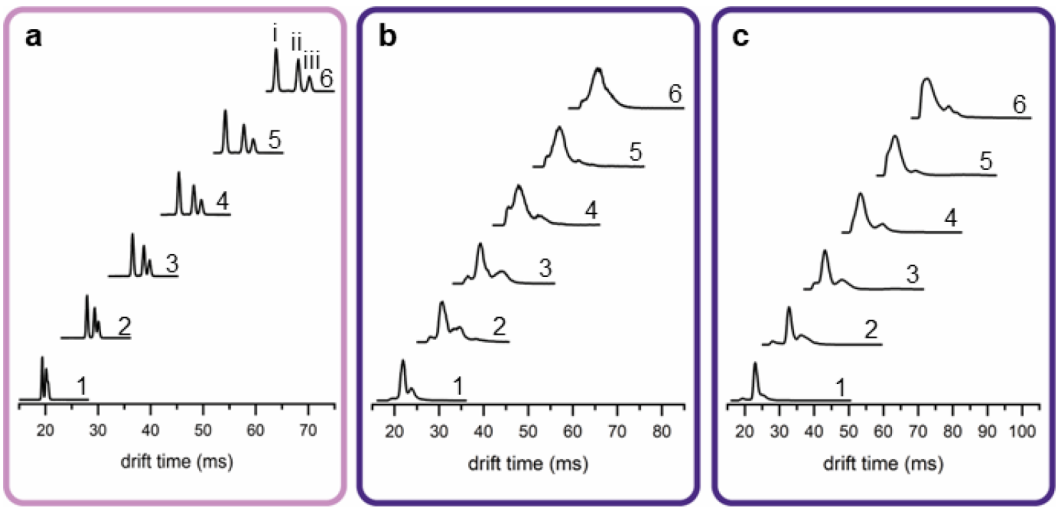

Figure 2. Ion mobility distributions recorded using a cyclic IMS instrument with increasing numbers of passes through the drift cell. Numbers to the right of each trace represent the number of passes through the drift cell that the ions have completed. (a) Distributions for a mixture of three trisaccharide isomers. Peaks corresponding to each isomer are labeled i, ii, and iii representing melezitose, raffinose, and maltotriose, respectively. (b) Distributions for the 17+ and (c) 16+ charge states of hemoglobin.

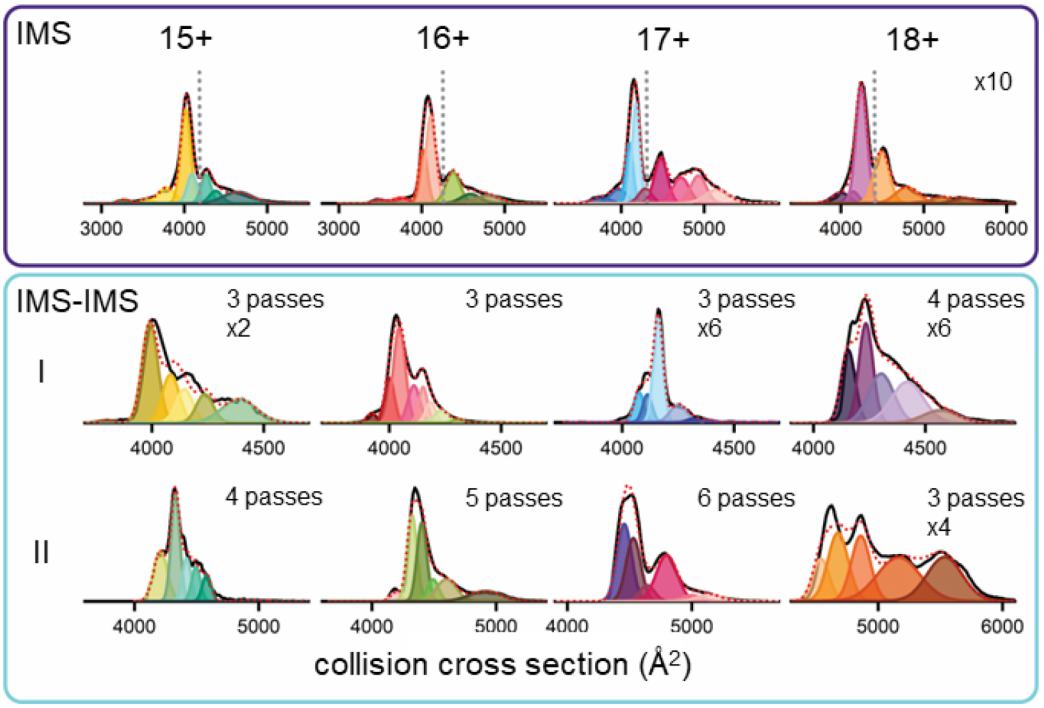

Figure 3. Total and selected mobility distributions for four charge states of hemoglobin. All total distributions are the result of a single pass through the cyclic mobility cell and selected distributions result from varying numbers of passes. For selected distributions, the number of passes includes the first pass prior to selection. The dotted gray lines in the total distributions represent the cutoff between selection I and selection II for each charge state. Some distributions have been magnified so that sufficient detail is visible. All distributions were measured at a solution temperature of 28 °C.

The same multipass separation technique was attempted for hemoglobin, and results for the 17+ and 16+ charge states are shown in Figure 2b and 2c, respectively. After a single pass, the distributions for both charge states appear to be similarly composed of a single main peak with smaller peaks to the left and right. Increasing the number of passes to two improves the separation as the smaller peaks begin to pull away from the main peak and new peaks start to emerge. This trend continues through three passes but is notably absent after four passes. At this point, the main peak and smaller peaks for both charge states have broadened to a degree that begins to erase the improvements in separation that were gained over the first three passes. The resolving power of the main peak of the 17+ charge state does not increase further after three passes while the resolving power of the main peak of the 16+ charge state reaches a maximum at four passes. Resolving power as a function of the number of passes for both charge states is plotted in Figure S7 and values are provided in Table S2. Any advances in separation are diminished as the number of passes is increased to five and six to the point where, after six passes, a

https://doi.org/10.1021/jasms.3c00032
J. Am. Soc. Mass Spectrom. 2023, 34, 1559−1568

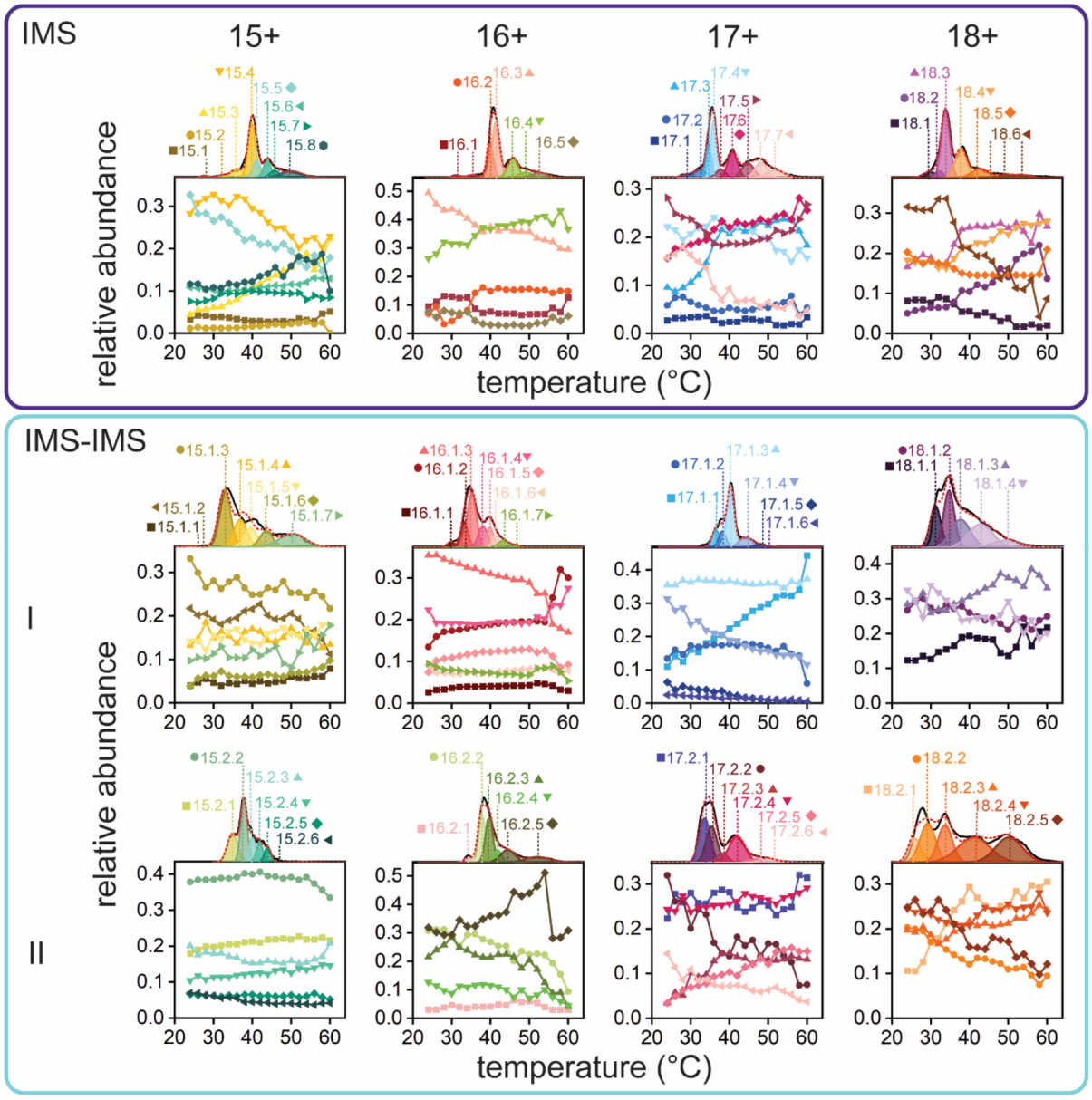

Figure 4. Relative abundances of conformations in the total and selected mobility distributions of hemoglobin as a function of temperature. A representative mobility spectrum (solution temperature of 28 °C) is provided at the top of each plot as a legend. All peaks are labeled according to the following scheme: charge state, selection number (where applicable), and sequential peak number. The numbers of passes for all experiments as well as the magnification on some distributions are the same as the values noted in Figure 3.

visual inspection reveals fewer peaks compared to the distributions after a single pass. Some broadening is expected in these mobility distributions because the ion packet becomes more diffuse after spending longer periods of time circulating in the drift cell. However, in the case of a protein such as hemoglobin, some of the observed broadening may also be caused by the separation of structures with subtle differences in cross section. These structures are not distinct after increasing the number of passes, but they can be examined through IMS-IMS experiments.

Selected Mobility Distributions. The results of selecting portions of the mobility distributions for each of the four charge states of hemoglobin at a solution temperature of 28 °C are presented in Figure 3. Two selections were obtained per charge state. The top portion of the figure shows the mobility spectrum of each charge state after a single pass through the drift cell. A gray dotted line in each of these distributions indicates where the region of the first selection ends and the second selection begins. These cuts were chosen to examine the main peak and the second most abundant peak of these distributions in separate distributions. The lower portion of the figure shows the mobility distribution for each pair of selections, labeled I and II. The total number of passes for each selection (including the original first pass) is noted for each spectrum along with the magnification where applicable. The number of passes for each selection was determined separately and maximized experimentally until further passes no longer yielded reasonable signal.

Most of the selected distributions have a similar shape compared to the regions in the total distributions from which they originate which indicates that the structures that give rise to the total distributions are still present in the selected

https://doi.org/10.1021/jasms.3c00032
J. Am. Soc. Mass Spectrom. 2023, 34, 1559−1568

distributions. However, more peaks are required to fit the selected data compared to the regions in the total distributions from which they originate. The most significant increase is observed in the first selection of the 16+ charge state. In the total spectrum, the region corresponding to this selection requires four peaks for an accurate fit. When this region is isolated and subjected to two additional passes to generate the spectrum for selection I, eight peaks are required to accurately model the data. Similar trends are observed across the remaining three charge states, resulting in an average increase of approximately two peaks in the selected data compared to the same regions in the original distribution. Interestingly, one selection does not show any increase in the number of peaks. Selection II of the 18+ charge state can be fit with five peaks which is the same number required for an accurate fit in this region of the total spectrum. This similarity suggests that five structures are present in this region of the total spectrum and, consequently, isolation and further separation does not reveal additional conformations.

In other cases, the selected distributions reveal structures that are necessary to model the total distributions but are not evident in the raw data. One prominent example is observed in the first selection of the 17+ charge state. In the total spectrum for this charge state, two peaks are necessary to fit the main peak because the peak maximum shifts to a slightly more compact cross section at higher solution temperatures (Figure S8). The raw data (black trace) provides no other indicators that the main peak is composed of two separate structures. However, when the main peak is isolated and further separated, the compact component of the peak not only becomes apparent but also increases in abundance at higher solution temperatures. The same phenomenon is observed in the 18+ charge state which also displays a comparable shift to a more compact cross section in the main peak without providing further evidence that this peak may represent more than one conformation. Selecting this peak generates the mobility spectrum provided in Figure 3, where the raw data indicates the presence of a compact conformation to the left of the main peak. The same trend is observed for the 16+ charge state but to a lesser extent. In this case, selecting the main peak does enhance the abundance of the compact population within the main peak but does not distinguish this peak in the mobility trace. The greater degree of structural heterogeneity within this selection may obfuscate the compact species as more conformations are separating and diffusing compared to the first selections of other charge states. The only charge state without a secondary compact portion in the main peak is the 15+ charge state, possibly because this charge state begins to decrease in abundance at relatively low solution temperatures which may inhibit the growth of any compact structures.

The distinction of species in selected distributions that are hinted at in the single pass data supports the accuracy of the Gaussian peak fitting model for defining structures in mobility distributions. This model, as well as the trend of an additional main peak within the total mobility distributions of hemoglobin, are further corroborated by the reproducibility of this result. All selected distributions are obtained in individual experiments that are separate from the collection of the total distributions which underpins the authenticity of the compact structures.

Temperature Dependence of Total and Selected Mobility Distributions. Variable temperature experiments were conducted to further compare structures in the total and selected mobility distributions. This technique has been used previously to characterize the relationship between solution and gas phase conformations of proteins.[30,37,82,90] The results of these experiments are presented in Figure 4. All conformations are labeled in the representative distributions according to charge state, selection number (where applicable), and sequential conformation number. Conformations with similar cross sections and changes as a function of temperature are assumed to arise from the same conformation in solution and have been grouped together.[30,37] Evidence for these groupings is provided in the Supporting Information (Figure S9), as are additional mobility distributions for each charge state at representative temperatures (Figures S8 and S10, respectively). The mobility distributions in Figure 4 are all obtained at a solution temperature of 28 °C for comparison across charge states, but more characteristic distributions for higher charge states are shown in Figure S8. The plethora of structures and temperature trends precludes a discussion of each individual conformation, so this discussion is focused on a selection of conformations that highlight overarching trends in the data set.

A comparison between the temperature dependencies of the total and selected distributions reveals a nuanced relationship. In many instances, the patterns exhibited by the most abundant peaks in the total distributions are predictive of trends in their selected counterparts. The main peak of the 15+ charge state, 15.4, decreases in abundance at higher temperatures as does conformation 15.1.3, the most abundant conformation in the first selection of the 15+ charge state. A similar correspondence occurs between the main peaks of the total and first selection of the 16+ charge state (16.3 and 16.1.3, respectively). The compact portion of this peak in the total spectrum (16.2) exhibits the opposite trend wherein the relative abundance increases with temperature. This trend is also echoed in the selected spectrum (16.1.2), and this relationship is maintained for the more compact portions of the main peaks in the 17+ and 18+ charge states (17.3 and 17.1.1, 18.2 and 18.1.1). Similar comparisons can be drawn for the more extended portions of the total distributions. The 16+ charge state displays an increase in the abundance of conformation 16.5, mirrored by the increase in conformation 16.2.5 in the second selection. In contrast, the most extended structures in the 18+ charge state (18.6) decrease at higher temperatures, but this pattern agrees with the decrease of conformation 18.2.5 in the second selection of this charge state. These general correlations in temperature dependence between total and selected distributions help to lay a framework for understanding how the additional structures that are present in the selected data may relate to structures in the original distributions.

A variation on this pattern that appears consistently throughout the relative abundance plots is that of structures in the selected distributions with abundances that change in the same manner as similar structures in the total data but at a different rate. This trend is apparent when comparing conformation 15.4 to conformation 15.1.3. The former comprises much of the main peak in the 15+ charge state and the latter is the most abundant peak in the first selection of the same charge state, so a similar structure likely contributes to both peaks and therefore some congruity in temperature dependence is expected. Both conformations decrease in abundance at higher solution temperatures, but the rate of decrease is much greater for 15.4 compared with 15.1.3. The

https://doi.org/10.1021/jasms.3c00032
J. Am. Soc. Mass Spectrom. 2023, 34, 1559−1568

same trend is observed when comparing the main peak in the 16+ charge state (16.3) to the main peak of the corresponding first selection (16.1.3), although the opposite trend occurs for the more compact portion of the main peak (16.2) compared to its counterpart (16.1.2). In the second case, both conformations increase in abundance as solution temperature increases, but 16.1.2 does not show a major increase until 56 °C, 20 °C beyond the point where 16.2 has completed its major thermal transition. The same pattern emerges when comparing conformation 17.3, the compact portion of the main peak in the 17+ charge state, to conformation 17.1.3. Both conformations increase in abundance at higher temperatures, but 17.3 undergoes a major transition which ends at 38 °C while the abundance of 17.1.3 increases steadily through 60 °C.

There are likely multiple factors that contribute to the observed differences in rates of change as a function of temperature. One possibility is that, as single conformations in the total distributions are pulled apart into multiple conformations in the selected distributions, the contributions of these new conformations to the temperature behavior in the total distributions also emerge. For example, conformation 17.5 shows a decrease in temperature up to 38 °C after which the abundance steadily increases. No conformations in either selection of the 17+ charge state show this exact temperature dependence. However, in selection II, conformation 17.2.2 decreases sharply in abundance through approximately 38 °C. At this point, its relative abundance is more similar to that of conformation 17.2.3. This conformation increases in abundance at higher temperatures. These two conformations may generate a combined temperature dependence that gives rise to the behavior observed for conformation 17.5.

Some conformations, in contrast, demonstrate little to no significant change as the solution is heated. Instead, their relative abundance remains constant across the temperature range. Such conformations are present across all charge states and include conformations 15.1, 16.1.6, 17.1.3, and 18.5. These structures may be the result of gas-phase activation at some stage in the mobility separation as they show no effects from changing solution temperature. The array portion of the cyclic drift cell is a potential source of this activation as this region must be raised to 70 V for ions to take the turn onto the racetrack (See instrument settings in Table S1). Lower voltages have not been sufficient to induce hemoglobin ions to take the turn required to enter the mobility cell and they pass through to the time-of-flight region with no separation. The required array voltage may be high enough to destabilize some structures which causes each charge state to exhibit certain conformations that do not change with solution temperature. Many of these conformations are also relatively low in abundance and may therefore be less energetically favorable which increases their propensity for further destabilization. These structures could also experience activation during the selection process. Ions may undergo collisions while they are trapped in the prestore region, leading to activated structures in the final spectrum. Further experiments are currently underway to examine how these instrumental aspects affect the observed temperature dependencies, or lack thereof.

Although some conformations in the selected distributions are not observed to change in abundance with increasing solution temperature, more temperature-dependent conformations can be observed for hemoglobin when the mobility distributions have been selected compared to a single pass containing all ions. In the total mobility distributions, 16 conformations change in relative abundance by 5% or more as the solution temperature increases from 24 to 60 °C. In the selected distributions, 24 structures meet this criterion over the same temperature range. Selection experiments appear to be capable of characterizing additional structures in ion mobility studies designed to uncover and investigate native and non-native protein conformations arising from solution structures.

SUMMARY AND CONCLUSIONS

Cyclic IMS-MS coupled with vT-ESI offers new possibilities for characterizing the conformational distributions of intact proteins by increasing the path length of the mobility separation. In the case of Hb, as the path length is extended, these improvements begin to decline as the IMS peaks appear to broaden. This phenomenon indicates that multiple unresolved species in a heterogeneous structural distribution are present, but unresolved. IMS-IMS selection experiments to isolate and further separate individual populations of ions have resolved many structures that were predicted to exist in the IMS distributions based on a Gaussian fitting model, which adds new justification for this method of data analysis. vT-ESI studies of these selections have shown that some conformations in the selected distributions change similarly with temperature compared to their counterparts in the original distributions, but some conformations change differently, which indicates that this technique can be used to uncover new structures from solution. Some trends, such as differences in the rate of change of relative abundance between total and selected distributions and the lack of temperature dependence for several conformations demonstrate that further studies of the effects of multipass and selective separations are necessary to fully understand the way that this instrument may affect protein structure in the gas phase. The results presented here provide a foundation for future cyclic IMS studies by demonstrating the capability of this instrument to examine protein structure with previously unseen detail.

ASSOCIATED CONTENT

Supporting Information

The Supporting Information is available free of charge at https://pubs.acs.org/doi/10.1021/jasms.3c00032.

Representative mass spectra, average charge state curve, relative abundance of tetramer and dimer, calibration curve, representative mobility distributions, representative IMS-IMS distributions, evidence for grouping, resolving power trends, explanation of IMS-IMS, instrument settings (PDF)

AUTHOR INFORMATION

Corresponding Author

David E. Clemmer − *Department of Chemistry, Indiana University Bloomington, Bloomington, Indiana 47405, United States;* orcid.org/0000-0003-4039-1360; Email: clemmer@indiana.edu

Authors

Edie M. Sharon − *Department of Chemistry, Indiana University Bloomington, Bloomington, Indiana 47405, United States*

https://doi.org/10.1021/jasms.3c00032
J. Am. Soc. Mass Spectrom. 2023, 34, 1559−1568

Lucas W. Henderson − *Department of Chemistry, Indiana University Bloomington, Bloomington, Indiana 47405, United States*

Complete contact information is available at: https://pubs.acs.org/10.1021/jasms.3c00032

Notes

The authors declare the following competing financial interest(s): DEC declares the following financial conflicts of interest: founder of Megadalton Solutions, a startup company developing charge detection mass spectrometry. EMS and LWH declare no competing financial conflicts of interest.

■ ACKNOWLEDGMENTS

This work is supported in part by grants from the National Institutes of Health R01 GM121751, 1R01GM131100-05, and 1R01GM135264.

■ REFERENCES

(1) Scheckel, C.; Aguzzi, A. Prions, prionoids and protein misfolding disorders. *Nat. Rev. Genet.* **2018**, *19* (7), 405−418.
(2) Pallarès, I.; Ventura, S. Understanding and predicting protein misfolding and aggregation: Insights from proteomics. *Proteomics* **2016**, *16* (19), 2570−2581.
(3) Nevone, A.; Merlini, G.; Nuvolone, M. Treating Protein Misfolding Diseases: Therapeutic Successes Against Systemic Amyloidoses. *Front. Pharmacol.* **2020**, *11*, 1−17.
(4) Schroeder, H. W., Jr.; Cavacini, L. Structure and function of immunoglobulins. *J. Allergy Clin. Immunol.* **2010**, *125* (2), S41−S52.
(5) Sonksen, P.; Sonksen, J. Insulin: understanding its action in health and disease. *Br. J. Anaesth.* **2000**, *85* (1), 69−79.
(6) Tokarz, V. L.; Macdonald, P. E.; Klip, A. The cell biology of systemic insulin function. *J. Cell Biol.* **2018**, *217* (7), 2273−2289.
(7) Ciechanover, A.; Heller, H.; Elias, S.; Haas, A. L.; Hershko, A. ATP-dependent conjugation of reticulocyte proteins with the polypeptide required for protein degradation. *Proc. Natl. Acad. Sci.* **1980**, *77* (3), 1365−1368.
(8) Glickman, M. H.; Ciechanover, A. The Ubiquitin-Proteasome Proteolytic Pathway: Destruction for the Sake of Construction. *Physiol. Rev.* **2002**, *82* (2), 373−428.
(9) Onuchic, J. N.; Wolynes, P. G. Theory of protein folding. *Curr. Opin. Struct. Biol.* **2004**, *14* (1), 70−75.
(10) Dill, K. A.; Ozkan, S. B.; Shell, M. S.; Weikl, T. R. The Protein Folding Problem. *Annu. Rev. Biophys.* **2008**, *37* (1), 289−316.
(11) Dill, K. A. Polymer principles and protein folding. *Protein Sci.* **1999**, *8* (6), 1166−1180.
(12) Daggett, V.; Fersht, A. The present view of the mechanism of protein folding. *Nat. Rev. Mol. Cell Biol.* **2003**, *4* (6), 497−502.
(13) Kelly, S. M.; Price, N. C. The application of circular dichroism to studies of protein folding and unfolding. *Biochim. Biophys. Acta* **1997**, *1338* (2), 161−185.
(14) Stryer, L. Fluorescence Spectroscopy of Proteins. *Science* **1968**, *162* (3853), 526−533.
(15) Barth, A. Infrared spectroscopy of proteins. *Biochim. Biophys. Acta* **2007**, *1767* (9), 1073−1101.
(16) Hellmann, N.; Schneider, D. Hands On: Using Tryptophan Fluorescence Spectroscopy to Study Protein Structure. In *Methods Mol. Biol.*; Springer: New York, 2019; pp 379−401.
(17) Rygula, A.; Majzner, K.; Marzec, K. M.; Kaczor, A.; Pilarczyk, M.; Baranska, M. Raman spectroscopy of proteins: a review. *J. Raman Spectrosc.* **2013**, *44* (8), 1061−1076.
(18) Jahnke, W.; Widmer, H. Protein NMR in biomedical research. *Cell. Mol. Life Sci.* **2004**, *61* (5), 580−599.
(19) Yee, A. A.; Savchenko, A.; Ignachenko, A.; Lukin, J.; Xu, X.; Skarina, T.; Evdokimova, E.; Liu, C. S.; Semesi, A.; Guido, V.; Edwards, A. M.; Arrowsmith, C. H. NMR and X-ray Crystallography, Complementary Tools in Structural Proteomics of Small Proteins. *J. Am. Chem. Soc.* **2005**, *127* (47), 16512−16517.
(20) Engen, J. R.; Botzanowski, T.; Peterle, D.; Georgescauld, F.; Wales, T. E. Developments in Hydrogen/Deuterium Exchange Mass Spectrometry. *Anal. Chem.* **2021**, *93* (1), 567−582.
(21) Engen, J. R.; Wales, T. E. Analytical Aspects of Hydrogen Exchange Mass Spectrometry. *Annu. Rev. Anal. Chem.* **2015**, *8* (1), 127−148.
(22) Kim, S. J.; Born, B.; Havenith, M.; Gruebele, M. Real-Time Detection of Protein-Water Dynamics upon Protein Folding by Terahertz Absorption Spectroscopy. *Angew. Chem., Int. Ed.* **2008**, *47* (34), 6486−6489.
(23) Kaltashov, I. A.; Eyles, S. J. Studies of biomolecular conformations and conformational dynamics by mass spectrometry. *Mass Spectrom. Rev.* **2002**, *21* (1), 37−71.
(24) Berman, H. M.; Westbrook, J.; Feng, Z.; Gilliland, G.; Bhat, T. N.; Weissig, H.; Shindyalov, I. N.; Bourne, P. E. The Protein Data Bank. *Nucleic Acids Res.* **2000**, *28* (1), 235−42.
(25) Stirling, P. C.; Lundin, V. F.; Leroux, M. R. Getting a grip on non-native proteins. *EMBO reports* **2003**, *4* (6), 565−570.
(26) Bohrer, B. C.; Merenbloom, S. I.; Koeniger, S. L.; Hilderbrand, A. E.; Clemmer, D. E. Biomolecule Analysis by Ion Mobility Spectrometry. *Annu. Rev. Anal. Chem.* **2008**, *1* (1), 293−327.
(27) Liu, Y.; Valentine, S. J.; Counterman, A. E.; Hoaglund, C. S.; Clemmer, D. E. Peer Reviewed: Injected-Ion Mobility Analysis of Biomolecules. *Anal. Chem.* **1997**, *69* (23), 728A−735A.
(28) Wang, G.; Bondarenko, P. V.; Kaltashov, I. A. Multi-step conformational transitions in heat-treated protein therapeutics can be monitored in real time with temperature-controlled electrospray ionization mass spectrometry. *The Analyst* **2018**, *143* (3), 670−677.
(29) Mirza, U. A.; Cohen, S. L.; Chait, B. T. Heat-induced conformational changes in proteins studied by electrospray ionization mass spectrometry. *Anal. Chem.* **1993**, *65* (1), 1−6.
(30) El-Baba, T. J.; Woodall, D. W.; Raab, S. A.; Fuller, D. R.; Laganowsky, A.; Russell, D. H.; Clemmer, D. E. Melting Proteins: Evidence for Multiple Stable Structures upon Thermal Denaturation of Native Ubiquitin from Ion Mobility Spectrometry-Mass Spectrometry Measurements. *J. Am. Chem. Soc.* **2017**, *139* (18), 6306−6309.
(31) El-Baba, T. J.; Clemmer, D. E. Solution thermochemistry of concanavalin A tetramer conformers measured by variable-temperature ESI-IMS-MS. *Int. J. Mass spectrom.* **2019**, *443*, 93−100.
(32) Muneeruddin, K.; Kaltashov, I. A.; Wang, G. Characterizing Soluble Protein Aggregates Using Native Mass Spectrometry Coupled with Temperature-Controlled Electrospray Ionization and Size-Exclusion Chromatography. In *Methods Mol. Biol.*; Springer: New York, 2022; pp 455−468.
(33) Woodall, D. W.; El-Baba, T. J.; Fuller, D. R.; Liu, W.; Brown, C. J.; Laganowsky, A.; Russell, D. H.; Clemmer, D. E. Variable-Temperature ESI-IMS-MS Analysis of Myohemerythrin Reveals Ligand Losses, Unfolding, and a Non-Native Disulfide Bond. *Anal. Chem.* **2019**, *91* (10), 6808−6814.
(34) Brown, C. J.; Woodall, D. W.; El-Baba, T. J.; Clemmer, D. E. Characterizing Thermal Transitions of IgG with Mass Spectrometry. *J. Am. Soc. Mass Spectrom.* **2019**, *30* (11), 2438−2445.
(35) Butler, K. E.; Takinami, Y.; Rainczuk, A.; Baker, E. S.; Roberts, B. R. Utilizing Ion Mobility-Mass Spectrometry to Investigate the Unfolding Pathway of Cu/Zn Superoxide Dismutase. *Front Chem* **2021**, *9*, 614595.
(36) El-Baba, T. J.; Raab, S. A.; Buckley, R. P.; Brown, C. J.; Lutomski, C. A.; Henderson, L. W.; Woodall, D. W.; Shen, J.; Trinidad, J. C.; Niu, H.; Jarrold, M. F.; Russell, D. H.; Laganowsky, A.; Clemmer, D. E. Thermal Analysis of a Mixture of Ribosomal Proteins by vT-ESI-MS: Toward a Parallel Approach for Characterizing the Stabilitome. *Anal. Chem.* **2021**, *93* (24), 8484−8492.
(37) Raab, S. A.; El-Baba, T. J.; Woodall, D. W.; Liu, W.; Liu, Y.; Baird, Z.; Hales, D. A.; Laganowsky, A.; Russell, D. H.; Clemmer, D. E. Evidence for Many Unique Solution Structures for Chymotrypsin Inhibitor 2: A Thermodynamic Perspective Derived from vT-ESI-

IMS-MS Measurements. *J. Am. Chem. Soc.* **2020**, *142* (41), 17372−17383.
(38) Ujma, J.; Jhingree, J.; Norgate, E.; Upton, R.; Wang, X.; Benoit, F.; Bellina, B.; Barran, P. Protein Unfolding in Freeze Frames: Intermediate States are Revealed by Variable-Temperature Ion Mobility−Mass Spectrometry. *Anal. Chem.* **2022**, *94* (35), 12248−12255.
(39) Shi, H.; Clemmer, D. E. Evidence for Two New Solu.tion States of Ubiquitin by IMS−MS Analysis. *J. Phys. Chem. B* **2014**, *118* (13), 3498−3506.
(40) Norgate, E. L.; Upton, R.; Hansen, K.; Bellina, B.; Brookes, C.; Politis, A.; Barran, P. E. Cold Denaturation of Proteins in the Absence of Solvent: Implications for Protein Storage**. *Angew. Chem.* **2022**, *134* (25), 1−6.
(41) Mao, Y.; Ratner, M. A.; Jarrold, M. F. Molecular Dynamics Simulations of the Rehydration of Folded and Unfolded Cytochrome c Ions in the Vapor Phase. *J. Am. Chem. Soc.* **2001**, *123* (27), 6503−6507.
(42) Shi, H.; Pierson, N. A.; Valentine, S. J.; Clemmer, D. E. Conformation Types of Ubiquitin [M+8H]8+ Ions from Water:-Methanol Solutions: Evidence for the N and A States in Aqueous Solution. *J. Phys. Chem. B* **2012**, *116* (10), 3344−3352.
(43) Gidden, J.; Bushnell, J. E.; Bowers, M. T. Gas-Phase Conformations and Folding Energetics of Oligonucleotides: dTG- and dGT-. *J. Am. Chem. Soc.* **2001**, *123* (23), 5610−5611.
(44) Gidden, J.; Ferzoco, A.; Baker, E. S.; Bowers, M. T. Duplex Formation and the Onset of Helicity in Poly d(CG)n Oligonucleotides in a Solvent-Free Environment. *J. Am. Chem. Soc.* **2004**, *126* (46), 15132−15140.
(45) Raab, S. A.; El-Baba, T. J.; Laganowsky, A.; Russell, D. H.; Valentine, S. J.; Clemmer, D. E. Protons Are Fast and Smart; Proteins Are Slow and Dumb: On the Relationship of Electrospray Ionization Charge States and Conformations. *J. Am. Soc. Mass Spectrom.* **2021**, *32* (7), 1553−1561.
(46) Breuker, K.; Mclafferty, F. W. Stepwise evolution of protein native structure with electrospray into the gas phase, 10^{-12} to 10^{2} s. *Proc. Natl. Acad. Sci.* **2008**, *105* (47), 18145−18152.
(47) Lee, S.-W.; Freivogel, P.; Schindler, T.; Beauchamp, J. L. Freeze-Dried Biomolecules: FT-ICR Studies of the Specific Solvation of Functional Groups and Clathrate Formation Observed by the Slow Evaporation of Water from Hydrated Peptides and Model Compounds in the Gas Phase. *J. Am. Chem. Soc.* **1998**, *120* (45), 11758−11765.
(48) McLafferty, F. W.; Castro, S.; Breuker, K. Multi-step evolution of protein conformation on electrospray into the gas phase. *Eur J Mass Spectrom (Chichester)* **2010**, *16* (3), 437−42.
(49) Breuker, K.; Oh, H.; Horn, D. M.; Cerda, B. A.; Mclafferty, F. W. Detailed Unfolding and Folding of Gaseous Ubiquitin Ions Characterized by Electron Capture Dissociation. *J. Am. Chem. Soc.* **2002**, *124* (22), 6407−6420.
(50) Oh, H.; Breuker, K.; Sze, S. K.; Ge, Y.; Carpenter, B. K.; Mclafferty, F. W. Secondary and tertiary structures of gaseous protein ions characterized by electron capture dissociation mass spectrometry and photofragment spectroscopy. *Proc. Natl. Acad. Sci.* **2002**, *99* (25), 15863−15868.
(51) Horn, D. M.; Breuker, K.; Frank, A. J.; Mclafferty, F. W. Kinetic Intermediates in the Folding of Gaseous Protein Ions Characterized by Electron Capture Dissociation Mass Spectrometry. *J. Am. Chem. Soc.* **2001**, *123* (40), 9792−9799.
(52) Skinner, O. S.; Mclafferty, F. W.; Breuker, K. How Ubiquitin Unfolds after Transfer into the Gas Phase. *J. Am. Soc. Mass Spectrom.* **2012**, *23* (6), 1011−1014.
(53) Steinberg, M. Z.; Elber, R.; Mclafferty, F. W.; Gerber, R. B.; Breuker, K. Early Structural Evolution of Native Cytochrome c after Solvent Removal. *ChemBioChem* **2008**, *9* (15), 2417−2423.
(54) Dodds, J. N.; Baker, E. S. Ion Mobility Spectrometry: Fundamental Concepts, Instrumentation, Applications, and the Road Ahead. *J. Am. Soc. Mass Spectrom.* **2019**, *30* (11), 2185−2195.
(55) Giles, K.; Pringle, S. D.; Worthington, K. R.; Little, D.; Wildgoose, J. L.; Bateman, R. H. Applications of a travelling wave-based radio-frequency-only stacked ring ion guide. *Rapid Commun. Mass Spectrom.* **2004**, *18* (20), 2401−2414.
(56) Shvartsburg, A. A.; Smith, R. D. Fundamentals of Traveling Wave Ion Mobility Spectrometry. *Anal. Chem.* **2008**, *80* (24), 9689−9699.
(57) Webb, I. K.; Garimella, S. V. B.; Tolmachev, A. V.; Chen, T.-C.; Zhang, X.; Norheim, R. V.; Prost, S. A.; Lamarche, B.; Anderson, G. A.; Ibrahim, Y. M.; Smith, R. D. Experimental Evaluation and Optimization of Structures for Lossless Ion Manipulations for Ion Mobility Spectrometry with Time-of-Flight Mass Spectrometry. *Anal. Chem.* **2014**, *86* (18), 9169−9176.
(58) Ibrahim, Y. M.; Hamid, A. M.; Deng, L.; Garimella, S. V. B.; Webb, I. K.; Baker, E. S.; Smith, R. D. New frontiers for mass spectrometry based upon structures for lossless ion manipulations. *The Analyst* **2017**, *142* (7), 1010−1021.
(59) Deng, L.; Ibrahim, Y. M.; Hamid, A. M.; Garimella, S. V. B.; Webb, I. K.; Zheng, X.; Prost, S. A.; Sandoval, J. A.; Norheim, R. V.; Anderson, G. A.; Tolmachev, A. V.; Baker, E. S.; Smith, R. D. Ultra-High Resolution Ion Mobility Separations Utilizing Traveling Waves in a 13 m Serpentine Path Length Structures for Lossless Ion Manipulations Module. *Anal. Chem.* **2016**, *88* (18), 8957−8964.
(60) Michelmann, K.; Silveira, J. A.; Ridgeway, M. E.; Park, M. A. Fundamentals of Trapped Ion Mobility Spectrometry. *J. Am. Soc. Mass Spectrom.* **2015**, *26* (1), 14−24.
(61) Giles, K.; Ujma, J.; Wildgoose, J.; Pringle, S.; Richardson, K.; Langridge, D.; Green, M. A Cyclic Ion Mobility-Mass Spectrometry System. *Anal. Chem.* **2019**, *91* (13), 8564−8573.
(62) Moseley, J. T.; Snuggs, R. M.; Martin, D. W.; Mcdaniel, E. W. Mobilities, Diffusion Coefficients, and Reaction Rates of Mass-Indentified Nitrogen Ions in Nitrogen. *Phys. Rev.* **1969**, *178* (1), 240−248.
(63) Glaskin, R. S.; Ewing, M. A.; Clemmer, D. E. Ion Trapping for Ion Mobility Spectrometry Measurements in a Cyclical Drift Tube. *Anal. Chem.* **2013**, *85* (15), 7003−7008.
(64) Rüger, C. P.; Le Maître, J.; Maillard, J.; Riches, E.; Palmer, M.; Afonso, C.; Giusti, P. Exploring Complex Mixtures by Cyclic Ion Mobility High-Resolution Mass Spectrometry: Application Toward Petroleum. *Anal. Chem.* **2021**, *93* (14), 5872−5881.
(65) McKenna, K. R.; Li, L.; Baker, A. G.; Ujma, J.; Krishnamurthy, R.; Liotta, C. L.; Fernández, F. M. Carbohydrate isomer resolution via multi-site derivatization cyclic ion mobility-mass spectrometry. *Analyst* **2019**, *144* (24), 7220−7226.
(66) Harrison, J. A.; Pruška, A.; Bittner, P.; Muck, A.; Cooper-Shepherd, D. A.; Zenobi, R. Advancing Cyclic Ion Mobility Mass Spectrometry Methods for Studying Biomolecules: Toward the Conformational Dynamics of Mega Dalton Protein Aggregates. *Anal. Chem.* **2022**, *94* (36), 12435−12443.
(67) Koeniger, S. L.; Merenbloom, S. I.; Valentine, S. J.; Jarrold, M. F.; Udseth, H. R.; Smith, R. D.; Clemmer, D. E. An IMS−IMS Analogue of MS−MS. *Anal. Chem.* **2006**, *78* (12), 4161−4174.
(68) Merenbloom, S. I.; Koeniger, S. L.; Valentine, S. J.; Plasencia, M. D.; Clemmer, D. E. IMS−IMS and IMS−IMS−IMS/MS for Separating Peptide and Protein Fragment Ions. *Anal. Chem.* **2006**, *78* (8), 2802−2809.
(69) Merenbloom, S. I.; Bohrer, B. C.; Koeniger, S. L.; Clemmer, D. E. Assessing the Peak Capacity of IMS−IMS Separations of Tryptic Peptide Ions in He at 300 K. *Anal. Chem.* **2007**, *79* (2), 515−522.
(70) Koeniger, S. L.; Merenbloom, S. I.; Clemmer, D. E. Evidence for Many Resolvable Structures within Conformation Types of Electrosprayed Ubiquitin Ions. *J. Phys. Chem. B* **2006**, *110* (13), 7017−7021.
(71) Deslignière, E.; Botzanowski, T.; Diemer, H.; Cooper-Shepherd, D. A.; Wagner-Rousset, E.; Colas, O.; Béchade, G.; Giles, K.; Hernandez-Alba, O.; Beck, A.; Cianférani, S. High-Resolution IMS−MS to Assign Additional Disulfide Bridge Pairing in Complementarity-Determining Regions of an IgG4 Monoclonal Antibody. *J. Am. Soc. Mass Spectrom.* **2021**, *32* (10), 2505−2512.

https://doi.org/10.1021/jasms.3c00032
J. Am. Soc. Mass Spectrom. 2023, 34, 1559−1568

(72) Eldrid, C.; Ben-Younis, A.; Ujma, J.; Britt, H.; Cragnolini, T.; Kalfas, S.; Cooper-Shepherd, D.; Tomczyk, N.; Giles, K.; Morris, M.; Akter, R.; Raleigh, D.; Thalassinos, K. Cyclic Ion Mobility−Collision Activation Experiments Elucidate Protein Behavior in the Gas Phase. *J. Am. Soc. Mass Spectrom.* **2021**, *32* (6), 1545−1552.
(73) Peterson, T. L.; Nagy, G. Toward Sequencing the Human Milk Glycome: High-Resolution Cyclic Ion Mobility Separations of Core Human Milk Oligosaccharide Building Blocks. *Anal. Chem.* **2021**, *93* (27), 9397−9407.
(74) Park, S.-Y.; Yokoyama, T.; Shibayama, N.; Shiro, Y.; Tame, J. R. H. 1.25 Å Resolution Crystal Structures of Human Haemoglobin in the Oxy, Deoxy and Carbonmonoxy Forms. *J. Mol. Biol.* **2006**, *360* (3), 690−701.
(75) Perutz, M. F. Stereochemistry of Cooperative Effects in Haemoglobin: Haem−Haem Interaction and the Problem of Allostery. *Nature* **1970**, *228* (5273), 726−734.
(76) Monod, J.; Wyman, J.; Changeux, J.-P. On the nature of allosteric transitions: A plausible model. *J. Mol. Biol.* **1965**, *12* (1), 88−118.
(77) Tame, J. R. What is the true structure of liganded haemoglobin? *Trends Biochem. Sci.* **1999**, *24* (10), 372−7.
(78) Lukin, J. A.; Kontaxis, G.; Simplaceanu, V.; Yuan, Y.; Bax, A.; Ho, C. Quaternary structure of hemoglobin in solution. *Proc. Natl. Acad. Sci. U.S.A.* **2003**, *100* (2), 517−520.
(79) Mueser, T. C.; Rogers, P. H.; Arnone, A. Interface sliding as illustrated by the multiple quaternary structures of liganded hemoglobin. *Biochemistry* **2000**, *39* (50), 15353−64.
(80) Safo, M. K.; Abraham, D. J. The Enigma of the Liganded Hemoglobin End State: A Novel Quaternary Structure of Human Carbonmonoxy Hemoglobin. *Biochemistry* **2005**, *44* (23), 8347−8359.
(81) Shibayama, N.; Sugiyama, K.; Tame, J. R. H.; Park, S.-Y. Capturing the Hemoglobin Allosteric Transition in a Single Crystal Form. *J. Am. Chem. Soc.* **2014**, *136* (13), 5097−5105.
(82) Woodall, D. W.; Brown, C. J.; Raab, S. A.; El-Baba, T. J.; Laganowsky, A.; Russell, D. H.; Clemmer, D. E. Melting of Hemoglobin in Native Solutions as measured by IMS-MS. *Anal. Chem.* **2020**, *92* (4), 3440−3446.
(83) Richardson, K.; Langridge, D.; Dixit, S. M.; Ruotolo, B. T. An Improved Calibration Approach for Traveling Wave Ion Mobility Spectrometry: Robust, High-Precision Collision Cross Sections. *Anal. Chem.* **2021**, *93* (7), 3542−3550.
(84) Ruotolo, B. T.; Benesch, J. L.; Sandercock, A. M.; Hyung, S. J.; Robinson, C. V. Ion mobility-mass spectrometry analysis of large protein complexes. *Nat Protoc* **2008**, *3* (7), 1139−52.
(85) Eldrid, C.; Ujma, J.; Kalfas, S.; Tomczyk, N.; Giles, K.; Morris, M.; Thalassinos, K. Gas Phase Stability of Protein Ions in a Cyclic Ion Mobility Spectrometry Traveling Wave Device. *Anal. Chem.* **2019**, *91* (12), 7554−7561.
(86) Haynes, S. E.; Polasky, D. A.; Dixit, S. M.; Majmudar, J. D.; Neeson, K.; Ruotolo, B. T.; Martin, B. R. Variable-Velocity Traveling-Wave Ion Mobility Separation Enhancing Peak Capacity for Data-Independent Acquisition Proteomics. *Anal. Chem.* **2017**, *89* (11), 5669−5672.
(87) Scarff, C. A.; Patel, V. J.; Thalassinos, K.; Scrivens, J. H. Probing hemoglobin structure by means of traveling-wave ion mobility mass spectrometry. *J. Am. Soc. Mass Spectrom.* **2009**, *20* (4), 625−631.
(88) Giles, K.; Williams, J. P.; Campuzano, I. Enhancements in travelling wave ion mobility resolution. *Rapid Commun. Mass Spectrom.* **2011**, *25* (11), 1559−66.
(89) Gaye, M. M.; Kurulugama, R.; Clemmer, D. E. Investigating carbohydrate isomers by IMS-CID-IMS-MS: precursor and fragment ion cross-sections. *The Analyst* **2015**, *140* (20), 6922−6932.
(90) Woodall, D. W.; Henderson, L. W.; Raab, S. A.; Honma, K.; Clemmer, D. E. Understanding the Thermal Denaturation of Myoglobin with IMS-MS: Evidence for Multiple Stable Structures and Trapped Pre-equilibrium States. *J. Am. Soc. Mass Spectrom.* **2021**, *32* (1), 64−72.

https://doi.org/10.1021/jasms.3c00032
J. Am. Soc. Mass Spectrom. 2023, 34, 1559−1568